Journal of Materials Science: Materials in Electronics (2020) 31:16830–16837
https://doi.org/10.1007/s10854-020-04237-2

Study of electrical properties of (Pr/Ca/Pb)MnO_3 ceramic

R. Hanen[1] · A. Mleiki[1,2] · H. Rahmouni[1] · N. Guermazi[3] · K. Khirouni[4] · A. Cheikhrouhou[2]

Received: 7 July 2020 / Accepted: 11 August 2020 / Published online: 20 August 2020

Abstract
Characterization of the electrical properties of $Pr_{0.65}Ca_{0.25}Pb_{0.1}MnO_3$ ceramic, prepared by the solid-state method, is conducted using the impedance spectroscopy technique. Ac-conductivity measurements reveal the presence of two electrical behaviors. A semiconductor character obtained at low-temperature ranges of 80–160 K, and a metallic behavior found at high-temperature ranges of 180–400 K. The temperature dependence of the exponent s confirms the contribution of two conduction processes in the transport mechanism. In the range of $T < 140$ K, the non-overlapping small polaron tunneling (NSPT) is the predominant mechanism. However, for $T > 140$ K, the conduction process is governed by the correlated barrier hopping (CBH) model. Finally, beyond $T = 250$ K, the dc-conductivity is characterized by the appearance of a saturation region.

1 Introduction

In the last decencies, manganese oxides have been extensively investigated in the scientific research field [1–3]. Such materials constitute a promising family of inorganic systems [4, 5]. Due to their unusual physical properties, manganites are used in enormous applications [6–8]. For examples, high electrical conductivity characteristic makes them functional for constructing solid oxide fuel cell (SOFC) [9, 10]. Owing to their important magnetocaloric effect and colossal magneto-resistance, manganites were explored in the magnetic cooling system, computer memory system, and magnetic sensors [11–14]. The physical properties of these systems can be improved by modifying several parameters, such as the nature of the dopant element, A-site deficiency, substitution sites, and preparation route [15–19]. In Ref [20], the studies of the praseodymium manganite ($PrMnO_3$) have demonstrated an interesting magnetic against Neel temperature (T_N). It exhibits antiferromagnetic insulator character at $T_N = 100$ K and anisotropic behavior at $T_N < 100$ K [21, 22]. Chukalkin et al. [23] have found that the contribution of lanthanum ion (La^{3+}) leads $LaMnO_3$ to be characterized by a weak ferromagnetic moment and by an inclined antiferromagnetic structure. The difference between the ionic radius of Pr^{3+} and La^{3+} allows Pr-based manganites to be the subject of material research [20]. From the magnetic analysis, $Pr_{1-x}Ca_xMnO_3$ compounds exhibit different behavior: ferromagnetic insulator for $x < 0.3$ and an antiferromagnetic charge ordering behavior for $x = 0.3$–0.5 [24]. Indeed, due to their multifunctional properties, $Pr_{1-x}Ca_xMnO_3$ entice the attention of many groups of research with calcium composition [8, 25–28]. It is important to mention that such systems have interesting electrical properties that allow them to be characterized by low-dimensional ferroelectricity [29]. Generally, for perovskite oxides, previous studies [30–33] have intensively investigated the electrical properties of such a material family. In the literature [34–37], experimental results have established that the physical properties of the manganite system can be influenced by the substitution at A-site. Such a substitution improves their electrical properties. Many works [18, 38, 39] have demonstrated that Pb-doping in manganite enhances the electrical conductivity. It is observed that the insertion of Pb in lanthanum-calcium manganite increases the cell volume, Curie temperature (T_C), as well as the electrical transition temperature [40]. In previous work, we have shown that the lowest obtained value

✉ A. Mleiki
alimlk1986@hotmail.com

1 Unité de Recherche Matériaux Avancés et Nanotechnologies (URMAN), Institut Supérieur des Sciences Appliquées et de Technologie de Kasserine, Kairouan University, BP 471, 1200 Kasserine, Tunisia

2 LT2S, Digital Research Center of Sfax, Sfax Technoparc, 3021 Sfax, Tunisia

3 Laboratoire Génie des Matériaux et Environnement (LGME), Ecole Nationale d'Ingénieurs de Sfax (ENIS), Université de Sfax, Sfax, Tunisia

4 Laboratoire de Physique des Matériaux et des Nanomatériaux appliquée à l'Environnement, Faculté des Sciences de Gabès cité Erriadh, Université de Gabès, 6079 Gabès, Tunisia

of the activation energy (E_a) corresponds to the Pb-doped $Pr_{0.65}Ca_{0.35}MnO_3$ [18]. Besides, dielectric results show that the $Pr_{0.65}Ca_{0.25}Pb_{0.1}MnO_3$ sample has better dielectric properties than Cd and Sr doped ones. Moreover, it has been observed that in $La_{0.7}Ca_{0.3-x}Pb_xMnO_3$ the electrical conductivity increases, and the metal–insulator transition temperature shifts towards higher temperatures [41]. Finally, of all the four samples $Pr_{0.67}A_{0.33}MnO_3$ (A = Ca, Sr, Pb, and Ba), it has been reported that $Pr_{0.67}Pb_{0.33}MnO_3$ compound is found to exhibit the highest magnetoresistance [42].

In this work, $Pr_{0.65}Ca_{0.25}Pb_{0.1}MnO_3$ ceramic was elaborated by solid-state reaction. Then, electrical properties are investigated.

2 Experimental details

$Pr_{0.65}Ca_{0.25}Pb_{0.1}MnO_3$ compound is prepared by conventional solid-state reaction using highly pure stoichiometry powders of Pr_6O_{11}, $CaCO_3$, $PbCO_3$, and MnO_2. During the process, the precursors were mixed and calcined at 900 °C for 12 h. Then, the obtained powder was pressed into pellets and sintered at 1000 and 1200 °C for 48 h. To conduct electrical measurements, a thin silver film was deposited through a circular mask of 6 mm of diameter on both sides of the pellet. Consequently, a configuration of a plate capacitor was obtained. Therefore, measurements of both electrical and dielectric properties were performed on an Agilent 4294A analyzer and Janis VPF800 cryostat. In addition, a wide range of frequency [40–10^8 Hz] and temperature [80–400 K] were used for measurements.

3 Results and discussions

3.1 X-ray diffraction

To determine the crystalline structure of $Pr_{0.65}Ca_{0.25}Pb_{0.1}MnO_3$, room temperature powder X-ray diffraction (XRD) pattern was collected and shown in Fig. 1. The Rietveld refinement of the XRD measurement suggests the sample belongs to the Pnma space group. The structural parameters of the unit cell are a = 5.4521 Å, b = 7.6886 Å and c = 5.4457 Å.

3.2 Ac-conductivity analysis

The ac-conductivity (σ_{ac}) spectra, at several temperature ranges of 80–100 K, 120–160 K, and 180–400 K for $Pr_{0.65}Ca_{0.25}Pb_{0.1}MnO_3$ are shown in Fig. 2a–c, respectively. In the temperature range of 80–100 K (Fig. 2a), two linear slopes were observed. Hence, the σ_{ac} can be described by Bruce equation [43–45]:

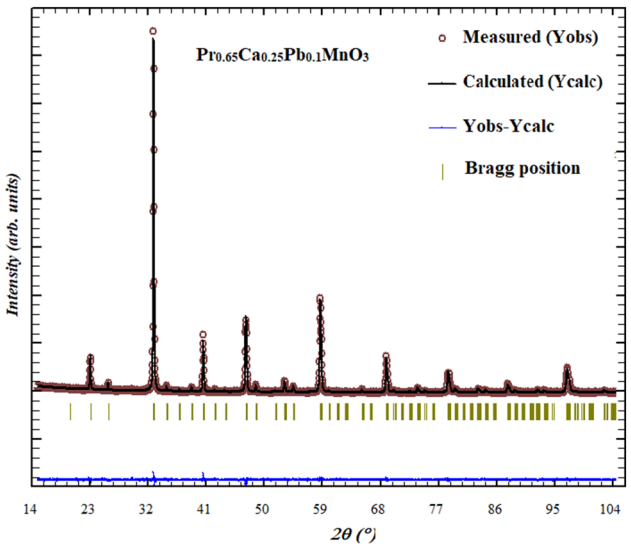

Fig. 1 Rietveld refined powder XRD pattern of the $Pr_{0.65}Ca_{0.25}Pb_{0.1}MnO_3$ compound

$$\sigma_{ac}(\omega) = \sigma_{dc} + A_1\omega^{S1} + A_2\omega^{S2} \quad (1)$$

where σ_{dc} is the dc-conductivity, A_1, A_2 are constants, s_1, and s_2 are the frequency exponents. Then, for the temperature range [120–160 K] (Fig. 2b), a large plateau appears at low-frequency corresponding to the σ_{dc}. Such behavior is accompanied by a change in slope at high frequency. So, the σ_{ac} can be expressed by the Jonsher law [43–45]:

$$\sigma_{ac}(\omega) = \sigma_{dc} + A\omega^{S1} \quad (2)$$

Beyond 180 K (Fig. 2c), a metallic behavior appears. Therefore, the conductivity response can be analyzed using the Drude model [46]:

$$\sigma_{AC} = \frac{\sigma_{DC}}{1 + (\omega\tau_s)^2} \quad (3)$$

where τ_s represents the relaxation time.

For the temperature dependence of the frequency exponent s, different models have been proposed [47, 48]. The variations of the exponent s_1 and s_2 as a function of temperature are shown in (Fig. 2d). From s_1 (T) plot, two different conduction mechanisms were determined: the non-overlapping small polaron tunneling (NSPT) [49, 50], and the correlated barrier hopping (CBH) mechanism [51–53]. The reported finding displays that the frequency exponent s_1 increases with the temperature until 140 K. This result indicates that the NSPT model is a suitable one to describe the conduction mechanism. In a covalent solid, if the incorporation of charge carriers to a site leads to a large degree of local lattice distortion, then the NSPT mechanism can be appeared [54]. According to this model,

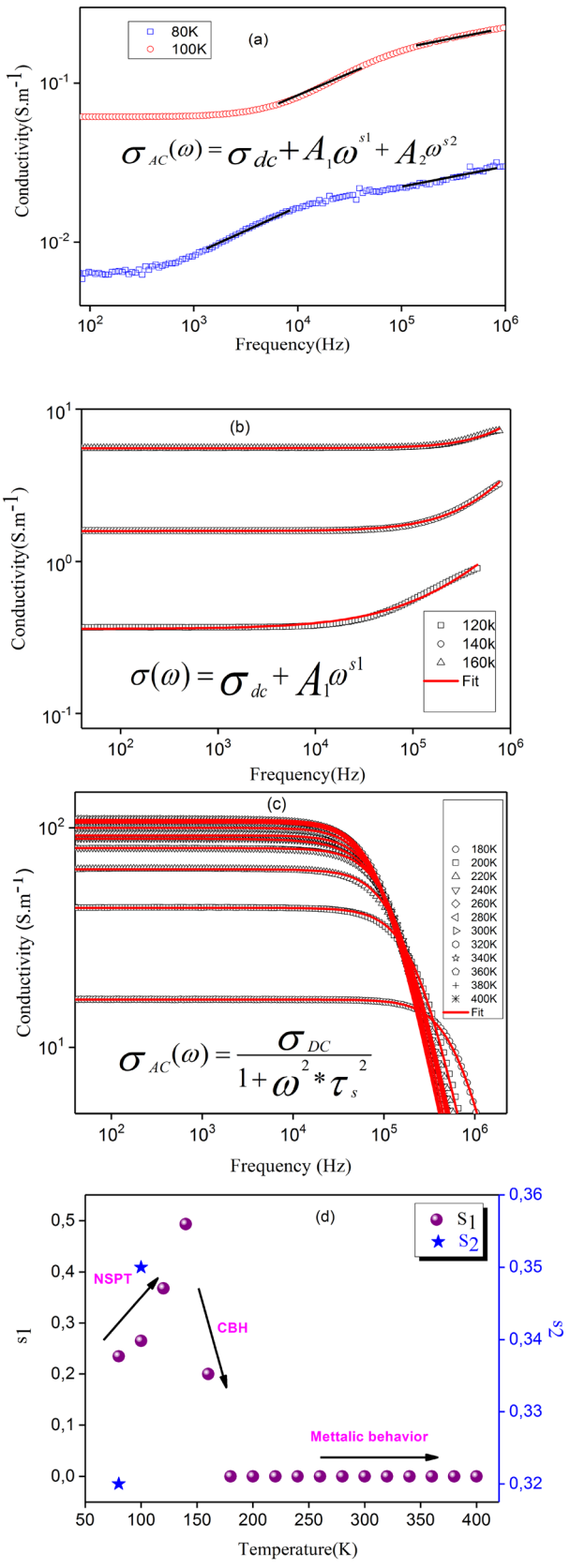

Fig. 2 Frequency dependence of ac-conductivity (σ_{ac}) for ▶ $Pr_{0.65}Ca_{0.25}Pb_{0.1}MnO_3$ compound at different temperatures ranges [80–100 K (**a**), 120–160 K (**b**) and 180–400 K (**c**)]. **d** Temperature dependence of the frequency exponent s_1 and s_2

the exponent s_1 can be described by the following expression [55]:

$$s_1 = 1 + \frac{4k_B T}{W_H} \tag{4}$$

where W_H is the polaron hopping energy.

For $T > 140$ K, s_1 decreases with increasing temperature. Consequently, the correlated barrier hopping (CBH) is the appropriate model to characterize the electrical conduction. According to this model, the conduction is generated by a polaron hopping mechanism trapped in two defect centers, over the Coulomb barrier that isolated it [55]. Then, the frequency exponent is described by the relation [55]:

$$s_1 = 1 - \frac{6k_B T}{W_m} \tag{5}$$

The variation of the second frequency exponent s_2 obtained at low-temperature increases with increasing temperature indicating that the NSPT is the adequate model for describing the conduction mechanism.

The evolution of ac-conductivity as a function of temperature at different frequencies for $Pr_{0.65}Ca_{0.25}Pb_{0.1}MnO_3$ is shown in Fig. 3a. The obtained result can be divided into two regions. In the first region (R-I), it is noticed that the conductivity increases with both temperature and frequency. Such variation can be related to the thermally enhanced drift mobility of charge carriers [56]. In the second region (R-II) and at low frequencies, a saturation region was detected. Then, a semiconductor–metal transition temperature was observed at $T = 180$ K for 400 kHz. Figure 3b shows the plot of $\sigma_{ac}.T$ versus $1000/T$ at different frequencies. The activation energies are deduced using the following relation [57]:

$$\sigma_{AC}.T = \sigma_0 \exp\left(\frac{-E_{ac}}{KT}\right) \tag{6}$$

At low frequencies, it is found that the activation energy values decrease with increasing frequency from $E_{a1} = 55$ meV to $E_{a1} = 44$ meV and from $E_{a2} = 137$ meV to $E_{a2} = 120$ meV at high and low temperature ranges, respectively. Such behavior confirms that the hopping conduction is the predominant mechanism [58, 59]. An increase in the applied field frequency leads to an improvement in electronic jumps between the localized states [60]. Hence, the activation energies decrease with increasing frequency. For 400 kHz, an only activation energy value was deduced $E_{a2} = 83$ meV,

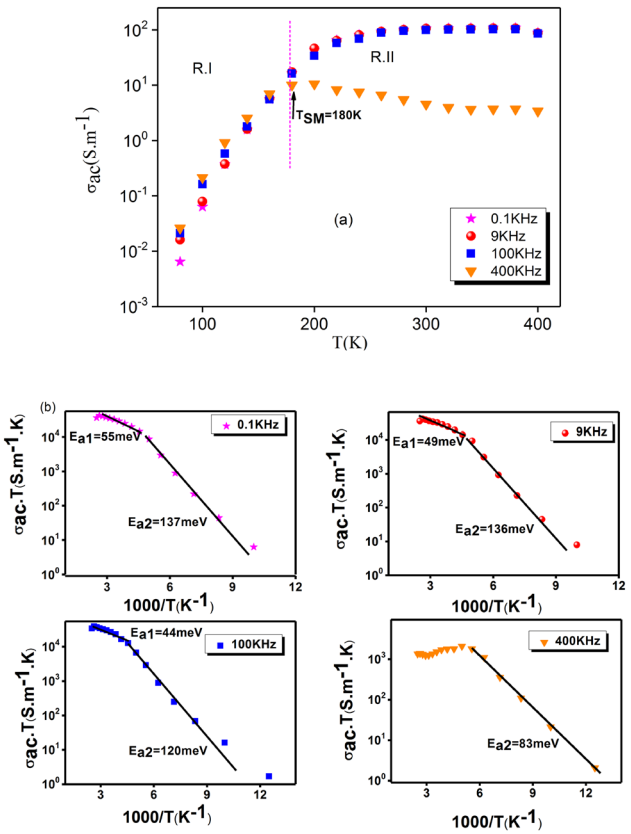

Fig. 3 **a** Variation of ac-conductivity (σ_{ac}) as a function of temperature at selected frequencies. **b** Variation of ($\sigma_{ac}.T$) versus (1000/T) for $Pr_{0.65}Ca_{0.25}Pb_{0.1}MnO_3$

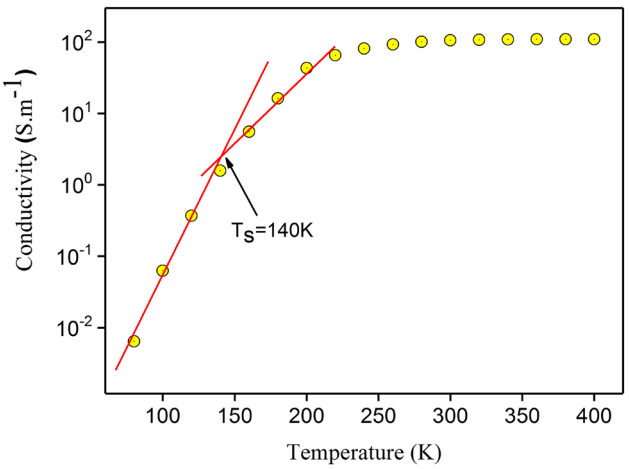

Fig. 4 Temperature dependence of the electrical conductivity $\sigma(T)$ of $Pr_{0.65}Ca_{0.25}Pb_{0.1}MnO_3$

confirming the appearance of metallic behavior (as previously reported in Fig. 3a).

3.3 Dc-conductivity analysis

The evolution of the dc-conductivity (σ_{dc}) as a function of temperature for $Pr_{0.65}Ca_{0.25}Pb_{0.1}MnO_3$ is shown in Fig. 4. As can be observed, the σ_{dc} increases with the temperature confirming a semiconductor behavior. Indeed, the increase in temperature provokes the increase of density of free carriers, which leads to the reduction of the encountered barriers and the improvement of electrical conductivity. At a specific temperature of T_{sat} = 250 K, the conductivity reaches a saturation region. This behavior suggests that the trapping centers are completely emptied. For T_s = 140 K, the change in slope can be related to the change in the conduction process.

3.4 Complex impedance analysis

The evolution of the real part of impedance (Z') versus frequency at different temperatures for the investigated compound is shown in Fig. 5a. The found result indicates higher values of Z' at low frequency. Then, it decreases with increasing temperature and frequency, suggesting an increase of the ac-conductivity [61]. Also, at high frequencies and for selected temperature, the merge of Z' confirms the presence of space charge polarization [62, 63]. From Z' spectrum, we can determine the Average Normalized Change (ANC). The temperature dependence of ANC for the investigated compound is illustrated in Fig. 5b. The ANC appears to be constant at low temperatures. Then, it decreases with temperature. Such evolution confirms the existence of different conduction mechanisms [64]. The variation of dANC/dT with temperature is illustrated in Fig. 5c. A change in the slope of dANC/dT was observed at T_{ANC} = 140 K, which is considered as a temperature at which the trapped centers seem to have vanished. The obtained temperature value is identical to the value evaluated from $\sigma_{dc}(T)$ curve ($T_{ANC} = T_s$) as shown in Fig. 4.

The normalization curve of Z''/Z''_{max} at different temperatures is shown in Fig. 6a. The spectrum is characterized by the appearance of a peak for each temperature. When the temperature increases, the peaks shift towards high frequencies, confirming the presence of a relaxation phenomenon. The observed peak does not lie at the same frequency. Such behavior specifies the non-Debye type of relaxation in our material [65]. Furthermore, for T = 80 K, we notice the presence of the second peak at high frequencies. This result proves the existence of the second relaxation.

At a fixed temperature, T = 100 K, for example, the variation of $d(Z'/Z'_{max})/df$ and Z''/Z''_{max} with frequency is shown in Fig. 6b. It is clear that the minimum of Z' and the maximum of Z'' do not merge, indicating the deviation from the Debye's model [65].

The Nyquist diagram is an exciting method to distinguish the contribution of the grains and grain boundary in the conduction mechanism and to model the sample by an

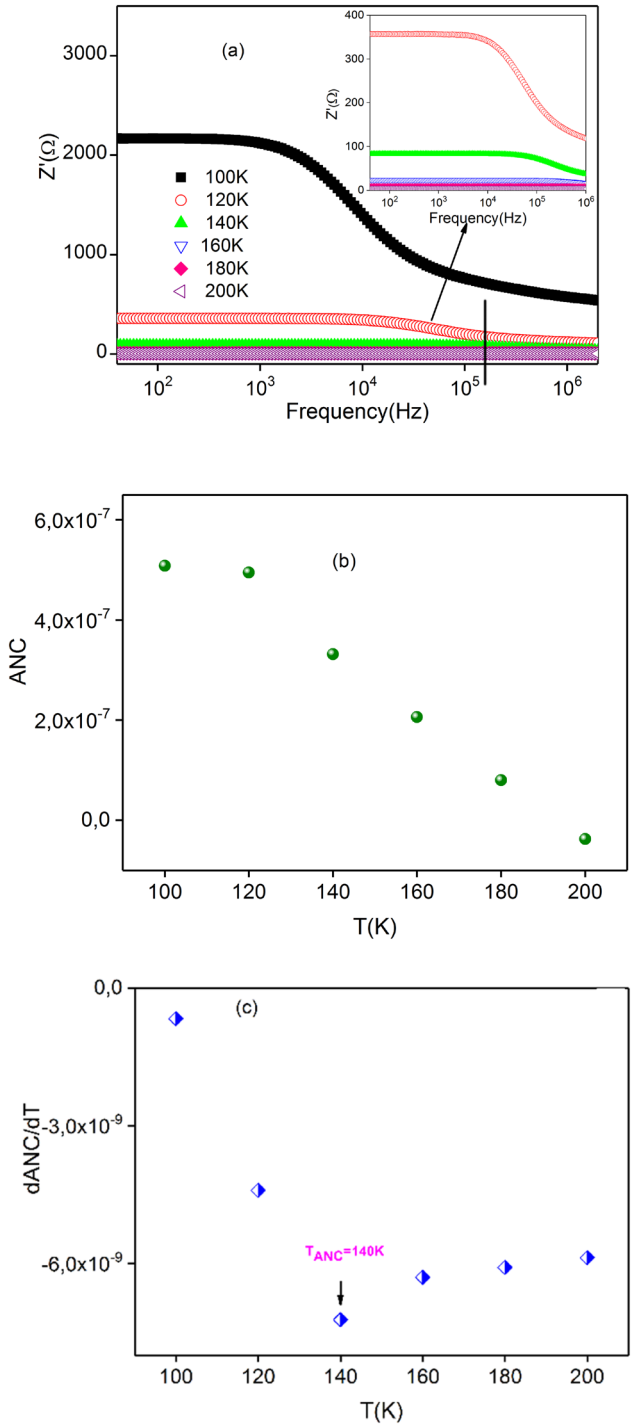

Fig. 5 **a** Evolution of Z' as a function of frequency at different temperatures for $Pr_{0.65}Ca_{0.25}Pb_{0.1}MnO_3$. **b**, **c** Temperature dependence of average normalized change (ANC) and dANC/dT

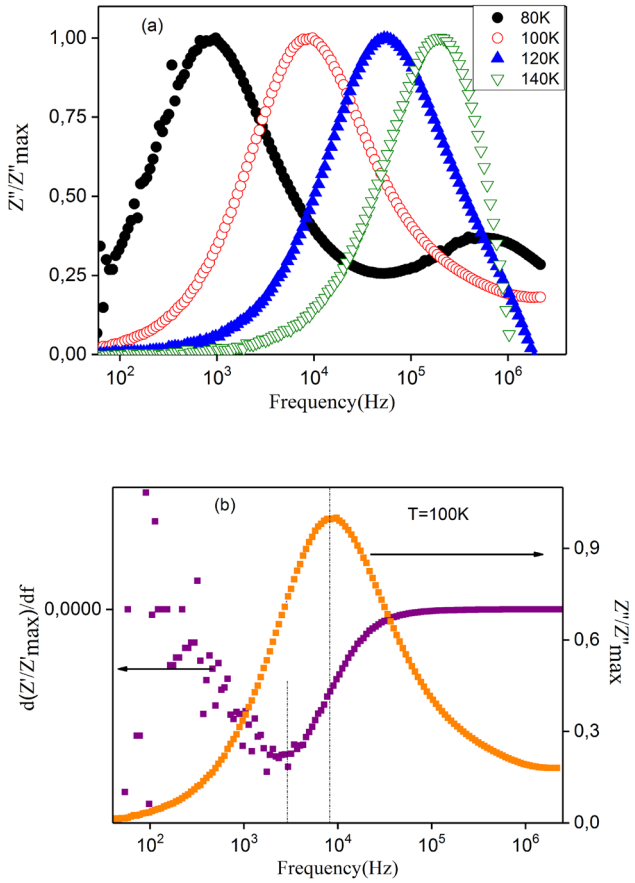

Fig. 6 **a** Variation of Z''/Z''_{max} versus frequency at different temperatures. **b** Frequency dependence of $d(Z'/Z'_{max})/df$ and Z''/Z''_{max} at $T = 100$ K for $Pr_{0.65}Ca_{0.25}Pb_{0.1}MnO_3$

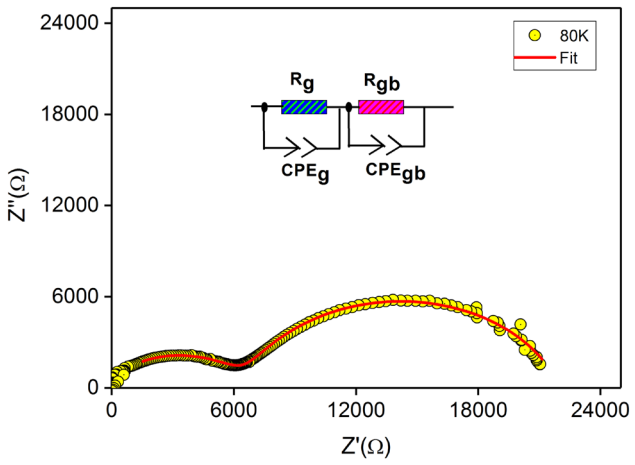

Fig. 7 Nyquist plot at $T = 80$ K for $Pr_{0.65}Ca_{0.25}Pb_{0.1}MnO_3$ compound

equivalent electrical circuit. In Fig. 7, we present the Nyquist diagram for $Pr_{0.65}Ca_{0.25}Pb_{0.1}MnO_3$ at $T = 80$ K. Two semi-circles are observed. At high frequencies, the semi-circle corresponds to the contribution of the grain. Then, at low frequencies, it represents the grain boundaries contribution [66]. The equivalent circuit is shown in the inset of Fig. 7 implying two parallel circuits: [Rg//CPEg] in series with a circuit [Rgb//CPEgb]. Rg and Rgb characterize the transport

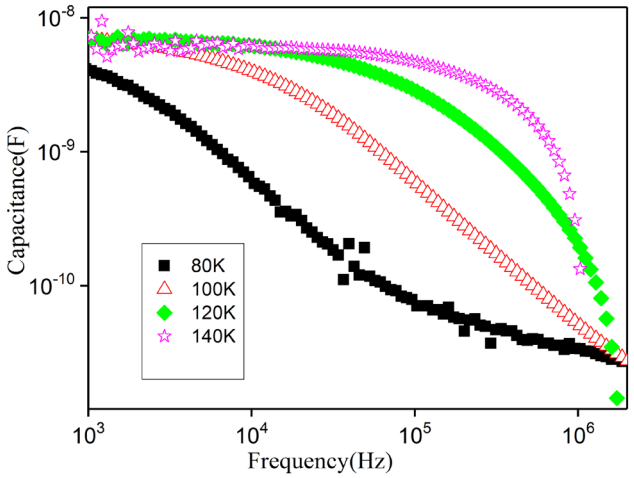

Fig. 8 Variation of the capacitance versus frequency at different temperatures for $Pr_{0.65}Ca_{0.25}Pb_{0.1}MnO_3$ compound

through grains and grain boundaries, respectively. The CPE impedance is determined by the following expression [67]: $Z_{CPE} = \frac{1}{Q(jw)^{\alpha}}$, where Q is the capacitance value of the CPE impedance, and α ($0 < \alpha < 1$) represents the deviation from Debye's model.

3.5 Dielectric study

The evolution of capacitance versus frequency at different temperatures for $Pr_{0.65}Ca_{0.25}Pb_{0.1}MnO_3$ ceramic is reported in Fig. 8. At low frequency, the capacitance increases with temperature, but it decreases with frequency. Based on the work of Bahgat and Abou-Zeid [68], the increase of the capacitance with temperature can be attributed to the reduction in bond energies. The same behavior was recently reported by M'nassri et al. [69]. In addition, the rise in temperature is followed by several effects. It reduces the interatomic forces, and it improves the orientational vibrations. On the other hand, an increase in temperature leads, as well known, to an increase in thermal agitation. Hence, the orientational vibrations are troubled. At high frequency, the capacitance sharply decreases. Such evolution may be due to the disappearance of space charges.

4 Conclusion

This paper presented an electrical characterization of $Pr_{0.65}Ca_{0.25}Pb_{0.1}MnO_3$ ceramics elaborated by the solid-state method. The admittance spectroscopy technique was used to conduct electrical measurements. It is found that the investigated ceramic exhibits a semiconductor behavior. In addition, a saturation region seems to appear at high temperatures ($T_{sat} = 250$ K). The ac-conductivity analysis indicates the presence of the hopping process. From such an analysis, the temperature dependence of the frequency exponent s suggests that the NSPT and CBH are the appropriate models to characterize the electrical conduction mechanisms. Then, complex impedance analysis proves the contribution of grains and grain boundaries in the conduction process and confirms the presence of a relaxation phenomenon. Also, dielectric properties are found to be strongly dependent on both temperature and frequency.

References

1. Y. Tomioka, T. Ito, A. Sawa, Electronic phase diagram of half-doped perovskite manganites on the plane of quenched disorder versus one-electron bandwidth. Phys. Rev. B **97**, 014409 (2018)
2. S. Dey, C. Rao, Splitting of CO_2 by manganite perovskites to generate CO by solar isothermal redox cycling. ACS Energy Lett. **1**, 237 (2016)
3. A. Mleiki, S. Othmani, W. Cheikhrouhou-Koubaa, A. Cheikhrouhou, E.K. Hlil, Normal and inverse magnetocaloric effect and short-range ferromagnetic interaction in $(Pr, Sm)_{0.5}Sr_{0.5}MnO_3$ phase separated manganite. J. Alloys Compd. **688**, 1214 (2016)
4. C. Reitz, P.M. Leufke, R. Schneider, H. Hahn, T. Brezesinski, Large magnetoresistance and electrostatic control of magnetism in ordered mesoporous $La_{1-x}Ca_xMnO_3$ thin films. Chem. Mater. **26**, 5745 (2014)
5. F. Borgatti, C. Park, A. Herpers, F. Offi, R. Egoavil, Y. Yamashita, A. Yang, M. Kobata, K. Kobayashi, J. Verbeeck, G. Panaccione, R. Dittmann, Chemical insight into electroforming of resistive switching manganite heterostructures. Nanoscale **5**, 3954 (2013)
6. Q. Yang, J. Yao, K. Zhang, W. Wang, X. Zuo, H. Tang, M. Wu, G. Li, Perovskite-type $La_{1-x}Ca_xMnO_3$ manganese oxides as effective counter electrodes for dye-sensitized solar cells. J. Electroanal. Chem. **833**, 1 (2019)
7. A. Mleiki, S. Othmani, W. Cheikhrouhou-Koubaa, M. Koubaa, A. Cheikhrouhou, E.K. Hlil, Effect of praseodymium doping on the structural, magnetic and magnetocaloric properties of $Sm_{0.55-x}Pr_xSr_{0.45}MnO_3$ ($0.1 < x < 0.4$) manganites. J. Alloys Compd. **645**, 559 (2015)
8. Y. Tokura, *Colossal Magnetoresistive Oxides* (Gordon and Breach Science, New York, 2000)
9. M. Pajot, V. Duffort, E. Capoen, A.S. Mamede, R.N. Vannier, Influence of the strontium content on the performance of $La_{1-x}Sr_xMnO_3/Bi_{1.5}Er_{0.5}O_3$ composite electrodes for low temperature solid oxide fuel cells. J. Power Sources **450**, 227649 (2020)
10. X. Lu, X. Yang, L. Jia, B. Chi, J. Pu, J. Li, First principles study on the oxygen reduction reaction of the $La_{1-x}Sr_xMnO_{3-\delta}$ coated $Ba_{1-x}Sr_xCo_{1-y}FeyO_{3-\delta}$ cathode for solid oxide fuel cells. Int. J. Hydrogen Energy **44**, 16359 (2019)
11. A. Mleiki, S. Othmani, W. Cheikhrouhou-Koubaa, A. Cheikhrouhou, E.K. Hlil, Enhanced relative cooling power in Ga-doped $La_{0.7}(Sr, Ca)_{0.3}MnO_3$ with ferromagnetic-like canted state. RSC Adv. **6**, 54299 (2016)
12. S. Tarhouni, A. Mleiki, I. Chaaba, H.B. Khelifa, W. Cheikhrouhou Koubaa, M. Koubaa, E.K. Hlil, Structural, magnetic and magnetocaloric properties of Ag-doped $Pr_{0.5}Sr_{0.5-x}Ag_xMnO_3$ manganites ($0.0 \le x \le 0.4$). Ceram. Int. **43**, 133 (2017)
13. A. Arabi, M. Fazli, M.H. Ehsani, Tuning the morphology and photocatalytic activity of $La_{0.7}Ca_{0.3}MnO_3$ nanorods via different

mineralizer-assisted hydrothermal syntheses. Mater. Res. Bull. **90**, 205 (2017)
14. F. Rahmani Afje, M.H. Ehsani, Size-dependent photocatalytic activity of $La_{0.8}Sr_{0.2}MnO_3$ nanoparticles prepared by hydrothermal synthesis. Mater. Res. Exp. **5**, 045012 (2018)
15. H. Rahmouni, B. Cherif, R. Jemai, A. Dhahri, K. Khirouni, Europium substitution for lanthanium in LaBaMnO—the structural and electrical properties of $La_{0.7-x}Eu_xBa_{0.3}MnO_3$ perovskite. J. Alloys Compd. **690**, 890 (2017)
16. H. Rahmouni, B. Cherif, M. Baazaoui, K. Khirouni, Effects of iron concentrations on the electrical properties of $La_{0.67}Ba_{0.33}Mn_{1-x}Fe_xO_3$. J. Alloys Compd. **575**, 9 (2013)
17. A. Mleiki, A. Khlifi, H. Rahmouni, N. Guermazi, K. Khirouni, A. Cheikhrouhou, Magnetic and dielectric properties of Balacunar $La_{0.5}Eu_{0.2}Ba_{0.3}MnO_3$ manganites synthesized using sol-gel method under different sintering temperatures. J. Magn. Magn. Mater. **502**, 166571 (2020)
18. R. Hanen, A. Mleiki, H. Rahmouni, N. Guermazi, K. Khirouni, E.K. Hlil, A. Cheikhrouhou, Effect of the nature of the dopant element on the physical properties of X-PrCaMnO system (X = Cd, Sr, and Pb). J. Magn. Magn. Mater. **508**, 166810 (2020)
19. B. Arun, V.R. Akshay, K.D. Chandrasekhar, G.R. Mutta, M. Vasundhara, Comparison of structural, magnetic and electrical transport behavior in bulk and nanocrystalline Nd-lacunar $Nd_{0.67}Sr_{0.33}MnO_3$ manganites. J. Magn. Magn. Mater. **472**, 74 (2019)
20. B. Christopher, A. Rao, B.S. Nagaraja, K.S. Prasad, G.S. Okram, G. Sanjeev, V.C. Petwal, V.P. Verma, J. Dwivedi, P. Poornesh, Correlation between structural and transport properties of electron beam irradiated $PrMnO_3$ compounds. Solid State Commun. **270**, 30 (2018)
21. J. Hemberger, M. Brando, R. Wehn, VYu Ivanov, A.A. Mukhin, A.M. Balbashov, A. Loidl, Magnetic properties and specific heat of $RMnO_3$ (R=Pr, Nd). Phys. Rev. B **69**, 64418 (2004)
22. K.B. Garg, M. Heinonen, P. Nordblad, S.D. Dalela, N. Panwar, V. Sen, S.K. Agarwal, N. Sharma, A comparative study of oxygen loss on in situ heating in $PrMnO_3$ and $BaMnO_3$. Int. J. Mod. Phys. B **25**, 1235 (2011)
23. Y. Chukalkin, A. Teplykh, B. Goshchitskii, Antiferro-ferromagnetic transformation in $LaMnO_3$ under neutron irradiation. Phys. Status Solidi B **242**, R70 (2005)
24. Y. Tomioka, A. Asamitsu, Y. Moritomo, Y. Tokura, Magnetic-field-induced metal-insulator phenomena in with controlled charge-ordering instability. Phys. Rev. B **53**, R1689 (1996)
25. T. Elovaara, H. Huhtinen, S. Majumdar, P. Paturi, Irreversible metamagnetic transition and magnetic memory in small-bandwidth manganite $Pr_{1-x}Ca_xMnO_3$ (x = 0.0–0.5). J. Phys.: Condens. Matter **24**, 216002 (2012)
26. Y. Tokura, Critical features of colossal magnetoresistive manganites. Rep. Prog. Phys. **69**, 797 (2006)
27. A.-M. Haghiri-Gosnet, J.-P. Renard, CMR manganites: physics, thin films and devices. J. Phys. D **36**, R127 (2003)
28. V.S. Kolat, T. Izgi, A.O. Kaya, N. Bayri, H. Gencer, S. Atalay, Metamagnetic transition and magnetocaloric effect in charge-ordered $Pr_{0.68}Ca_{0.32-x}Sr_xMnO_3$ (x = 0, 0.1, 0.18, 0.26 and 0.32) compounds. J. Magn. Magn. Mater. **322**, 427 (2010)
29. L.A. Dubraja, D. Wang, T. Brezesinski, Synthesis, structural characterization and magnetic properties of ordered mesoporous $Pr_{1-x}Ca_xMnO_3$ thin films. Cryst. Eng. Commun **20**, 245 (2018)
30. H. Rahmouni, B. Cherif, R. Jemai, A. Dhahri, K. Khirouni, Europium substitution for lanthanium in LaBaMnO—the structural and electrical properties of $La_{0.7-x}Eu_xBa_{0.3}MnO_3$ perovskite. J. Alloys Compd. **690**, 890 (2017)
31. A. Mleiki, R. Hanen, H. Rahmouni, N. Guermazi, K. Khirouni, E.K. Hlil, A. Cheikhrouhou, Study of magnetic and electrical properties of $Pr_{0.65}Ca_{0.25}Ba_{0.1}MnO_3$ manganite. RSC Adv. **8**, 31755 (2018)
32. A. Khlifi, A. Mleiki, H. Rahmouni, N. Guermazi, K. Khirouni, A. Cheikhrouhou, Barium deficiency and sintering temperature effects on structural and transport properties of $La_{0.5}Eu_{0.2}Ba_{0.3-x}MnO_3$ manganites. J. Mater. Sci: Mater. Electron. **30**, 19513 (2019)
33. N. Kharrat, R. Lahouli, W. Cheikhrouhou-Koubaa, L. Sicard, K. Khirouni, M. Koubaa, A. Cheikhrouhou, Effect of nickel doping on the electrical conductance properties of $La_{0.67}Ba_{0.33}Mn_{1-x}Ni_xO_3$ (x = 0 and 0.075) manganite. Solid State Commun. **297**, 21 (2019)
34. C. Saravanan, R. Thiyagarajan, P.V. Kanjariya, P. Sivaprakash, J.A. Bhalodia, S. Arumugam, Electrical resistivity, magnetic and magneto-caloric studies on perovskite manganites $Nd_{1-x}Cd_xMnO_3$ (x = 0 and 0.1) polycrystals. J. Magn. Magn. Mater. **476**, 35 (2019)
35. N. Choudhary, M.K. Verma, N.D. Sharma, S. Sharma, D. Singh, Correlation between magnetic and transport properties of rare earth doped perovskite manganites $La_{0.6}R_{0.1}Ca_{0.3}MnO_3$ (R = La, Nd, Sm, Gd, and Dy) synthesized by Pechini process. Mater. Chem. Phys. **242**, 122482 (2020)
36. M.K. Verma, N.D. Sharma, S. Sharma, N. Choudhary, D. Singh, Structural and magneto-transport properties of Li-substituted $La_{0.65}Ca_{0.35-x}Li_xMnO_3$ ($0 \le x \le 0.15$) CMR manganites. J. Alloys Compd. **814**, 152279 (2020)
37. X. Pu, H. Li, G. Dong, K. Chu, S. Zhang, Y. Liu, X. Liu, Electrical transport properties of $(Pr_{1-x}La_x)_{0.7}Sr_{0.3}MnO_3$ ($0 \le x \le 0.3$) polycrystalline ceramics prepared by sol-gel process for potential room temperature bolometer use. Ceram. Int. **46**, 4984 (2020)
38. N. Chau, H.N. Nhat, N.H. Luong, D.L. Minh, N.D. Tho, N.N. Chau, Structure, magnetic, magnetocaloric and magnetoresistance properties of $La_{1-x}Pb_xMnO_3$ perovskite. Phys. B **327**, 270 (2003)
39. A. Staneva, Y. Dimitriev, Y. Ivanova, E. Kashchieva, J.M. Viera, M. Kolev, Phase formation and microstructure of the $La_{0.6}Pb_{0.4}MnO_3$ obtained by low temperature methods. J. Univ. Chem. Technol. Metall. **42**, 55 (2007)
40. P. Phong, N. Khien, N. Dang, D. Manh, L. Hong, I.-J. Lee, Effect of pb substitution on structural and electrical transport of $La_{0.7}Ca_{0.3-x}Pb_xMnO_3$ ($0 \le x \le 0.3$) manganites. Phys. B **466**, 44 (2015)
41. P.T. Phong, N.V. Khien, N.V. Dang, D.H. Manh, L.V. Hong, I.-J. Lee, Effect of Pb substitution on structural and electrical transport of $La_{0.7}Ca_{0.3-x}Pb_xMnO_3$ ($0 \le x \le 0.3$) manganites. Phys. B **466**, 44 (2012)
42. D.C. Krishna, P. Venugopal Reddy, Magnetic transport behavior of nano-crystalline $Pr_{0.67}A_{0.33}MnO_3$ (A = Ca, Sr, Pb and Ba) manganites. J. Alloys Compd. **479**, 661 (2009)
43. P. Bruce, High and low frequency Jonscher behavior of an ionically conducting glass. Solid State Ion. **15**, 247 (1985)
44. S.R. Elliott, F.E.G. Henn, Application of the Anderson-Stuart model to the AC conduction of ionically conducting materials. J. Non-Cryst. Solids **116**, 179 (1990)
45. A.K. Jonscher, M.S. Frost, Weakly frequency-dependent electrical conductivity in a Chalcogenide glass. Thin Solid Films **37**, 267 (1976)
46. K. Lee, S. Cho, S.H. Park, Z.J. Heeger, C.-W. Lee, S.-H. Lee, Metallic transport in polyaniline. Nature **441**, 65 (2006)
47. W. Hzez, R. Hamdi, S. Kraiem, H. Rahmouni, A. Tozri, K. Khirouni, E. Dhahri, Close look on the impact of treating dysprosium manganite with Ca/Sr in terms of transport properties. J. Alloys Compd. **834**, 155121 (2020)
48. S. Rabha, P. Dobbidi, The impact of thickness on the optical, electrical and dielectric properties of nanocrystalline 0.9 MTO-0.1BNO composite thin films. Appl. Surf. Sci. **489**, 831 (2019)
49. A. Ghosh, Frequency-dependent conductivity in bismuth-vanadate glassy semiconductors. Phys. Rev. B **41**, 1479 (1990)

50. A. Ghosh, Transport properties of vanadium germanate glassy semiconductors. Phys. Rev. B **42**, 5665 (1990)
51. S. Mollah, K.K. Som, K. Bose, B.K. Chaudhuri, ac conductivity in $Bi_4Sr_3Ca_3Cu_yO_x$ ($y = 0$–5) and $Bi_4Sr_3Ca_{3-z}Li_zCu_4O_x$ ($z = 0.1$–1.0) semiconducting oxide glasses. J. Appl. Phys. **74**, 931 (1993)
52. Y. Ben Taher, A. Oueslati, N.K. Maaloul, K. Khirouni, M. Gargouri, Conductivity study and correlated barrier hopping (CBH) conduction mechanism in diphosphate compound. Appl. Phys. A **120**, 1537 (2015)
53. V. Chithambaram, S. Jerome Das, S. Krishnan, Synthesis, optical and dielectric studies on novel semi organic nonlinear optical crystal by solution growth technique. J. Alloys Compd. **509**, 4543 (2011)
54. F. Gaâbel, M. Khlifi, N. Hamdaoui, K. Taibi, J. Dhahri, Conduction mechanisms study in $CaCu_{2.8}Ni_{0.2}Ti_4O_{12}$ ceramics sintered at different temperatures. J. Alloys Compd. **828**, 154373 (2020)
55. S.R. Elliott, A.c. conduction in amorphous chalcogenide and pnictide semi-conductors. Adv. Phys. **36**, 135 (1987)
56. B.P. Jacob, S. Thankachan, S. Xavier, E.M. Mohammed, Dielectric behavior and AC conductivity of Tb^{3+} doped $Ni_{0.4}Zn_{0.6}Fe_2O_4$ nanoparticles. J. Alloys Compd. **541**, 29 (2012)
57. N.F. Mott, E.A. Davis, *Electronic Process in Non-Crystalline Materials* (Clarendon Press, Oxford, 1979)
58. M. Okutan, E. Basaran, H.I. Bakan, F. Yakuphanoglu, AC conductivity and dielectric properties of Co-doped TiO_2. Phys. B **364**, 300 (2005)
59. S. Mahaboob, G. Prasad, G.S. Kumar, Electrical conduction in $(Na_{0.125}Bi_{0.125}\ Ba_{0.65}Ca_{0.1})(Nd_{0.065}Ti_{0.87}Nb_{0.065})O_3$ ceramic. Bull. Mater. Sci. **29**, 35 (2006)
60. ShA Mansour, I.S. Yahia, F. Yakuphanoglu, The electrical conductivity and dielectric properties of C.I. Basic Violet 10. Dyes Pigm. **87**, 144 (2010)
61. T. Rhimi, M. Toumi, K. Khirouni, S. Guermazi, AC conductivity, electric modulus analysis of $KLi(H_2PO_4)_2$ compound. J. Alloys Compd. **714**, 546 (2017)
62. J. Suchanicz, The low-frequency dielectric relaxation $Na_{0.5}Bi_{0.5}TiO_3$ ceramics. Mater. Sci. Eng. B **55**, 114 (1998)
63. A.R. James, K. Srinivas, Low temperature fabrication and impedance spectroscopy of PMN-PT ceramics. Mater. Res. Bull. **34**, 1301 (1999)
64. R. Jemaï, R. Lahouli, S. Hcini, H. Rahmouni, K. Khirouni, Investigation of nickel effects on some physical properties of magnesium based ferrite. J. Alloys Compd. **705**, 340 (2017)
65. W. Ncib, A. Ben Jazia Kharrat, M. Saadi, K. Khirouni, N. Chniba-Boudjada, W. Boujelben, Structural, AC conductivity, conduction mechanism and dielectric properties of $La_{0.62}Eu_{0.05}Ba_{0.33}Mn_{0.85}Fe_{0.15}O_3$ ceramic compound. J. Mater. Sci: Mater. Electron. **30**, 18391 (2019)
66. J.E. Bauerle, Study of solid electrolyte polarization by a complex admittance method. J. Phys. Chem. Solids **30**, 2657 (1969)
67. A.K. Jonscher, The interpretation of non-ideal dielectric admittance and impedance diagrams. Phys. Status Solidi A **32**, 665 (1975)
68. A.A. Bahgat, Y.M. Abou-Zeid, Mixed alkali effect in the K_2O–Na_2O–TeO_2 glass system. Phys. Chem. Glasses **42**, 01 (2001)
69. R. M'nassri, M. Khelifi, H. Rahmouni, A. Selmi, K. Khirouni, N. Chniba-Boudjada, A. Cheikhrouhou, Study of physical properties of cobalt substituted $Pr_{0.7}Ca_{0.3}MnO_3$ ceramics. Ceram. Int. **42**, 6145 (2016)